Molecular Crystals and Liquid Crystals
Publication details, including instructions for authors and subscription information:
http://www.tandfonline.com/loi/gmcl18

Nematic Liquid Crystal Sensors

Yu. V. Bocharov [a] , I. N. Gurova [a] , O. A. Kapustina [a] , E. I. Remizova [a] & V. N. Reshetov [a]
[a] Institute of Acoustics, Moscow, 117036, USSR
Version of record first published: 24 Sep 2006.

To cite this article: Yu. V. Bocharov , I. N. Gurova , O. A. Kapustina , E. I. Remizova & V. N. Reshetov (1991): Nematic Liquid Crystal Sensors, Molecular Crystals and Liquid Crystals, 209:1, 19-30

To link to this article: http://dx.doi.org/10.1080/00268949108036176

Mol. Cryst. Liq. Cryst., 1991, Vol. 209, pp. 19–30
Reprints available directly from the publisher
Photocopying permitted by license only

Printed in the United States of America

Nematic Liquid Crystal Sensors

YU. V. BOCHAROV, I. N. GUROVA, O. A. KAPUSTINA, E. I. REMIZOVA and V. N. RESHETOV

Institute of Acoustics Moscow 117036, USSR

(Received July 27, 1990)

Development of applied aspects of acoustooptic (AO) signal conversion theory in nematic liquid crystals[1] (NLC) resulted in creation of a new family of the sensors operating on the common physical principle and capable to follow variations of a number of physical values: pressure $P(t)$, vibrational velocities (linear $\xi(t)$ and angular $\Omega(t)$), temperature fluctuations $T(t)$.

Keywords: sensor, pressure, temperature fluctuations, vibrational velocity, acoustooptics

Operational scheme of such NLC sensor is shown in Figure 1. Here 1 is a sensitive cell (SC) of the sensor, filled with NLC 2; 3, light-emitting diode; 4, photodiode†; 5, communication line and 6, quantum electronic module. The basic link is the SC, which construction and elements base depend on the type of the action being measured.

The new sensors are constructed on the scheme of light polarization modulation by NLC layer. A periodic variation of the layer optical transmittance is caused by director oscillations in nematic hydrodynamic flow, which immediately results from either pressure oscillations at the SC input (in detectors of variable pressure and temperature fluctuations), or from the forces of inertia (in detectors of vibrational velocities). Generalized scheme of the conversion has the next form:

$$\varkappa_i(t) \rightarrow V(z, t) \rightarrow \varphi(z, t) \rightarrow \phi(t) \rightarrow I(t) \tag{1}$$

Function $\varkappa_i(t)$ assumes here the value of one of the parameters being measured, $V(z, t)$ is nematic liquid oscillating flow, $\varphi(z, t)$ - director oscillations angle, $\phi(t)$ - phase difference of ordinary and extraordinary light beams, $I(t)$ - intensity of light at the sensor output. In quasi-linear regime of conversion in a frequency band satisfying to inequality

$$\omega_H = (15/2)(\alpha_4 + \alpha_5)/\rho d^2 >> \omega >> \omega_L = \pi^2 K_3/\gamma_1 d^2, \tag{2}$$

the value $I(t)$ is related with parameter $\varkappa_i(t)$ as follows[2]:

$$I(t) = I_0(1 + A_i \varkappa_i(t)), \tag{3}$$

† Shown in Figure 1 light-emitting diode and photodiode may be removed from the SC case.

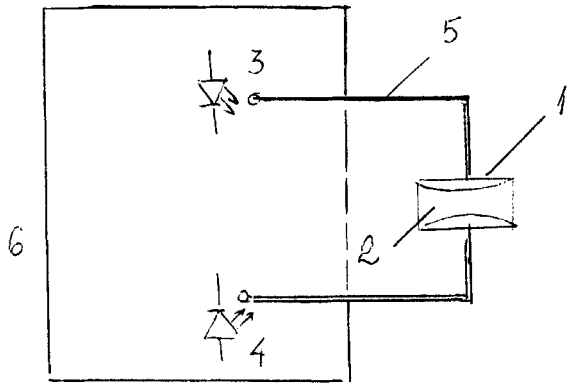

FIGURE 1

where the conversion coefficient A_i assumes the values, corresponding to the parameter being measured, I_0 - intensity of light incident at NLC layer; ρ and α_i, γ_1 - NLC density and viscous coefficients; K_3 - Frank elastic constant and d - NLC layer thickness in the plane section of the capillary.

Let us discuss the construction principles of different sensors types and their main technical characteristics.

VARIABLE PRESSURE SENSOR

In Figure 2(a) and (b) there are presented the schemes of two modifications of variable pressure sensor SC. Here 1 is a capillary with symmetrical horn-like edges, 2 - membranes M and 3 - a chamber of volume V_0. These modifications differ by a magnitude of an input acoustical impedance Z, equal

$$Z_1 = Z_0 + Z_M \text{ (first modification)}$$

$$Z_2 = Z_0 + Z_V \text{ (second modification)} \quad (4)$$

where respectively
$Z_0 = 12\,\eta_{ef}L/d^2$, $Z_V(\omega) = bd\rho_0 c_0^2/i\omega V_0$, $Z_M(\omega) = 6E\delta_M{}^3 bd/i\pi\omega R_M^4$ - acoustical impedances of the capillary, of the chamber and of the membrane,‡ ρ_0 and c_0 - density of liquid, filling the chamber, and sound velocity in it, δ_M and R_M - thickness and radius of the membrane, E - Young's modulus of the membrane material, η_{ef} - NLC effective viscousity, L and b - length and width of the capillary, d - its thickness in the plane section. The signal conversion follows the scheme (see Equa-

‡ Additional units (membranes M, chamber V_0) shown in Figure 2a and b change the input acoustical impedance Z_0 of the capillary to the values Z_1 and Z_2, which provides compensation of frequency dependent reaction of the SC itself on the signal being measured; this reaction is caused by not NLC peculiarity as anisotropic medium, but by a character of nematic viscous flow in the capillary: the amount of nematic, flowing during oscillation period, varies as $1/\omega$.[3]

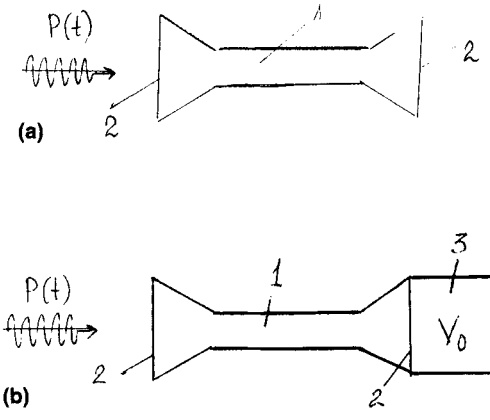

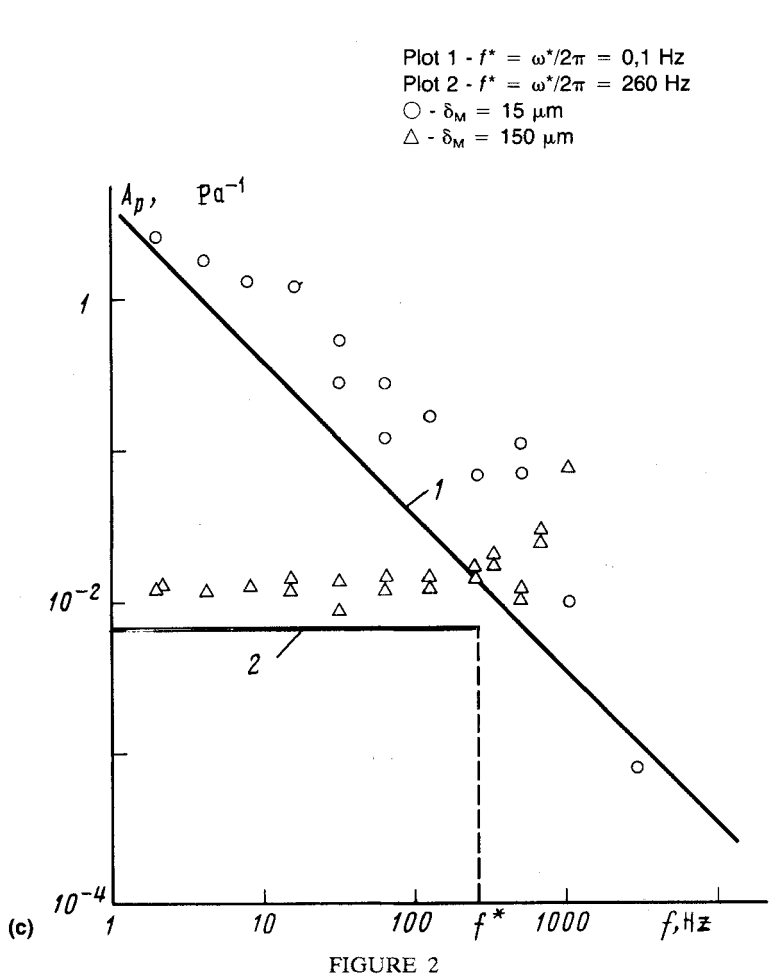

FIGURE 2

tion 1) and light intensity at the sensor output is defined from Equation (3), where $\varkappa_i(t) = P(t)$ and the conversion coefficient A_i equals

$$A_P = \pi^{1/2} d((1/2 + m)\Delta n k_0 d)^{1/2}/3^{1/2}\, \eta_{ef} L\omega^*. \tag{5}$$

Here Δn is NLC birefringence, k_0 – wave number of light, $m = 0; 1; 2; \ldots$ - conversion index, ω^* - the upper frequency, limiting the band where acoustical impedance is mainly elastic one, and the optical response of the sensor to variable pressure doesn't depend upon frequency. These boundary frequencies are equal to:

$$\omega_1^* = bd^3\rho_0 c_0^2/12\, \eta_{ef} L V_0 \qquad \text{(second modification)},$$

$$\omega_2^* = E\delta_M^3 d^2/\eta_{ef} L R_M^4 \qquad \text{(first modification)}. \tag{6}$$

In Figure 2(c), there are presented the results of calculations of the conversion coefficients for the first modification, carried out according Equations (5) and (6) for the following conditions: $L = 10^{-3}m$, $d = 10^{-4}m$, $b = 10^{-2}m$, $k_0 = 10^7\, m^{-1}$, $\Delta n = 0.25$, $\eta_{ef} = 0.05$ Pa.s, $m = 0$. Frequency band is 1 . . . 4000 Hz, the boundary frequencies $f^* = \omega^*/2\pi$ equal 0.1 and 260 Hz (plots 1 and 2, respectively).

Symbols 1 and 2 illustrate the data obtained while testing the SC of identical dimensions but with different values of input impedance:

$$Z_{M_1}/Z_{M_2} \simeq (\delta_{M_1}/\delta_{M_2})^3 \simeq 10^3;$$

membranes thicknesses δ_M and δ_{M_2} equaled 15 and 150 μm, respectively. It is seen, that agreement between theory and experiment is rather good. For the SC with high input impedance when the value of f^* gets into the testing frequency band, coefficient A_P follows the expression (5) and remains constant up to $f^* = 260$ Hz, as is determined by the theory. For the SC with low input impedance the conversion coefficient drops as $1/f$ which is also in agreement with the theory, because in this case $f^* = 0.1$ Hz and is out of the frequency band, being tested.

The experimental data presented above were obtained by comparison of the sensor with traditional calibrated Brûel & Kjaer hydrophone. The sensors SC were filled with NLC of the type N-8 (eutectic mixture of MBBA and EBBA).

TEMPERATURE FLUCTUATIONS SENSOR

The scheme of the temperature fluctuations sensor is shown in Figure 3(a). Here 1 is a capillary with symmetric horn-like edges; 2 and 3 - chambers of volume V_0; 4 - an air cavity of volume v.

Principle of the sensor functioning is the following: temperature fluctuations in surrounding medium are transmitted to NLC, filling the capillary and the chambers,

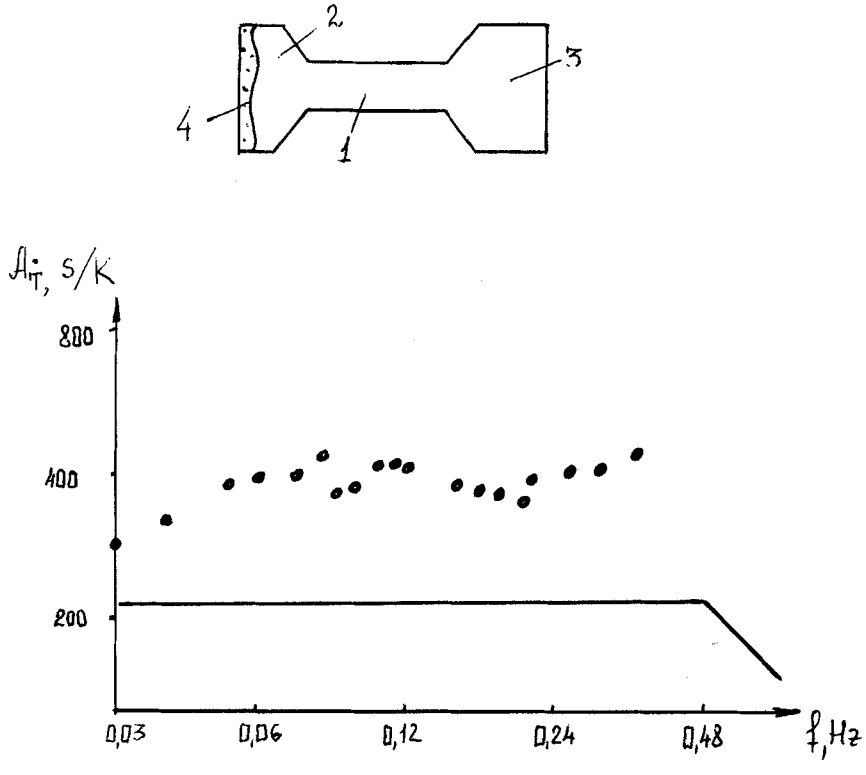

FIGURE 3

and cause fluctuations of NLC temperature and volume. This in turn gives rise to appearance of variable pressure at the SC input:

$$P(t) \simeq \beta_L/\rho c^2 T(t), \tag{7}$$

where β_L is NLC thermal expansion coefficient. The signal conversion scheme differs from the scheme (in Equation 1) only at the initial stage, which has the next form:

$$\varkappa_i(t) = T(t) \rightarrow P(t). \tag{8}$$

In accordance with that the relation of value $T(t)$ with light intensity at the sensor output is determined by Equation (3), where the function $\varkappa_i(t)$ and coefficient A_i assume the values of $T(t)$ and A_T. The analysis shows that the sensor temperature conversion coefficient is equal to:

$$A_T = V_0(\Delta n k_0 d(1/2 + m))^{1/2} \beta_L/bd^2, \tag{9}$$

when $\omega_L < \omega < \omega_H$,

and
$A_T = V_0 (\Delta n k_0 d(1/2 + m))^{1/2} \beta_L \omega/\omega_L b d^2 = A_{\dot{T}} \cdot \omega$,
when $\omega < \omega_L$, $\dot{T}$ - rate of temperature change, $A_{\dot{T}}$ – conversion coefficient related to $\dot{T}$.

In Figure 3(b) we present the results of the temperature conversion coefficient calculations, made according Equation (9) for the temperature oscillations frequency in the region of 10^{-3} . . . 10^2 Hz. The sensor dimensions are the same as for the pressure variations sensor. The chamber volume is $V_0 = 1$ cm^3, the conversion index $m = 0$. Physical parameters of NLC Δn, α_i, γ_1, K_3 correspond to the temperature 40°C.

It is easily seen that in low frequency band ($\omega < \omega_L$) the conversion coefficient grows up with increasing of temperature oscillations frequency. This follows from the fact, that NLC behaviour in that band is determined by NLC elasticity, rather than by its viscousity. At these frequencies the sensor registrates temperature fluctuations velocity $\partial T/\partial t$, rather than these fluctuations value $T(t)$, as at frequencies $\omega > \omega_L$.

In Figure 3(b) there are also shown the results of preliminary testing of the sensor, filled with NLC N-8, carried out by means of comparison with calibrated Fe-Constantan thermopair. These measurements were made in temperature interval of 30 . . . 50°C, and temperature fluctuations amplitude didn't exceed 0.1°C when $f = 0.03$ Hz and reduced to 0.01°C when $f = 0.4$ Hz. The chamber volume $V_0 = 1$ cm^3, and the air cavity volume $v \simeq 0.1$ cm^3. Insufficient sensitivity of the thermopair in the frequency band of temperature oscillations above 0.5 Hz made it impossible to obtain reliable data about the conversion coefficient A_T at these frequencies. However the measurements showed that the sensor has confidently registrated temperature oscillations up to 50 Hz. As it seen the qualitative agreement between theory and experiment is good. The quantitive comparison of these data is not seemed to be useful because of the absence of the precise values of the physical parameters of nematic mixture being used in the experiment, such as Δn, α_i, γ_1, K_3, related to the temperature of 40°C.

LINEAR VIBRATIONAL VELOCITY SENSOR

This sensor SC scheme is shown in Figure 4(a). Here 1 is a capillary with horn-like edges; 2, chambers and 3, membranes.

Operational principle is the next: vibrational velocity $\dot{\xi}(t)$ at the expense of inertia forces $\rho H \ddot{\xi}(t)$, depending on the height H of NLC column, results in variable pressure at the SE input:

$$P(t) \simeq \rho H \omega \dot{\xi}(t), \tag{10}$$

which causes according Equation (1) oscillations of reading radiation intensity. Respectively, the relation of the signal being measured $\dot{\xi}(t)$ with light intensity at the sensor output is defined from Equation (3), where $\varkappa_i(t) = \dot{\xi}(t)$, $A_i = A_{\dot{\xi}}$. The

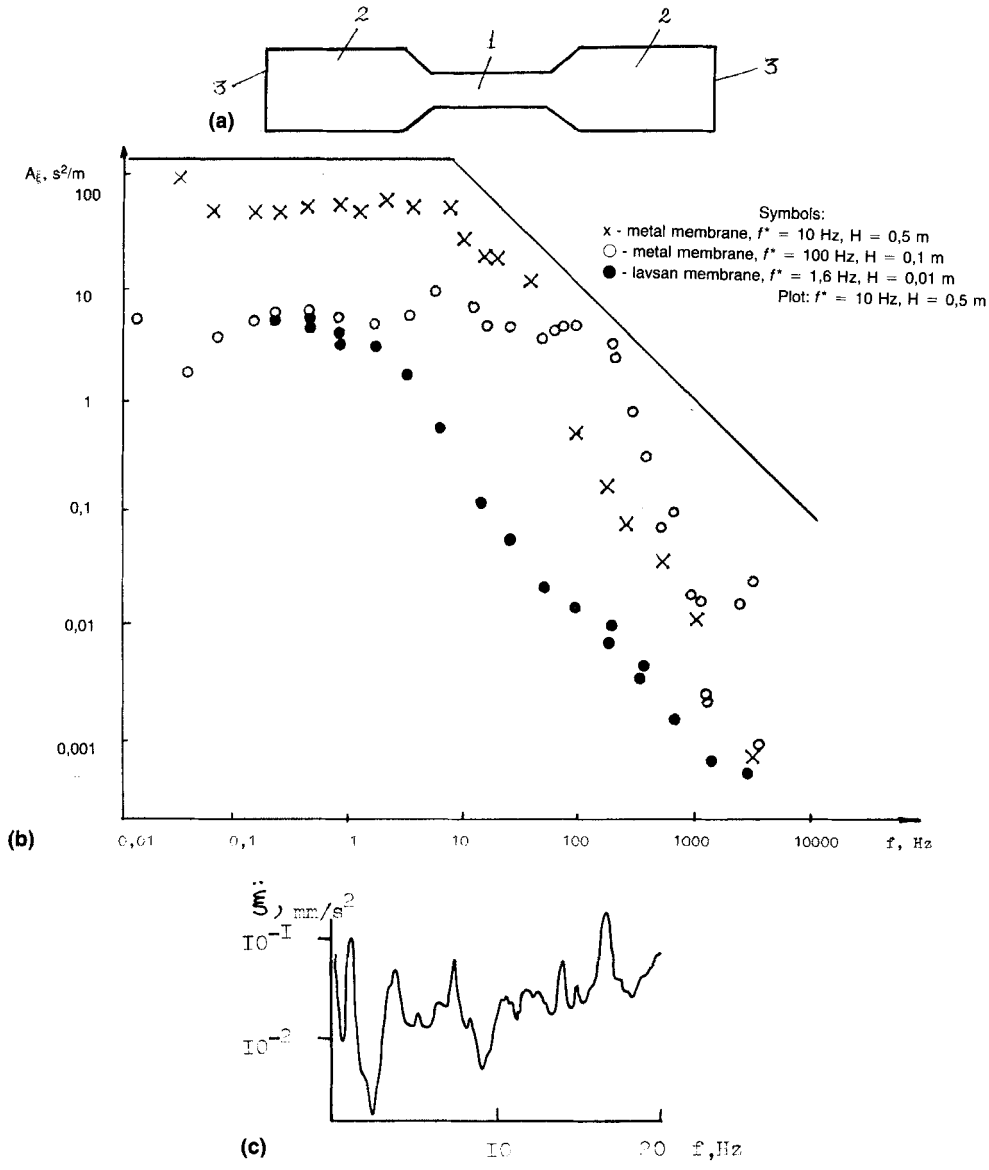

FIGURE 4

linear velocity conversion coefficient thus equals:

$$A_\xi = \rho H d(\Delta n k_0 d(1/2 + m))^{1/2}/\eta_{ef} L,$$

when

$$\omega_L^* < \omega < \omega_H, \tag{11}$$

and

$$A_{\ddot{\xi}} = \rho H d(\Delta n k_0 d(1/2 + m))^{1/2}\, \omega/\omega_L^*\, \eta_{ef} L = A_{\ddot{\xi}} \cdot \omega,$$

when $\omega < \omega_L^*$, $\ddot{\xi}$ - acceleration, $A_{\ddot{\xi}}$ - linear acceleration conversion coefficient. Here ω_L^* assumes the maximum value of the two: ω_L and ω_2^* (see Equations (2) and (6)) in accordance with the SC construction peculiarities.

A plot in Figure 4(b) presents the results of the linear acceleration conversion coefficient calculations, carried out from Equation (11) for oscillations frequencies band of 0.03 . . . 6000 Hz.

Geometrical dimensions of the sensor are: $H = 0.5\ m$, $d = 10^{-4} m$, $L = 10^{-3}$ m and $f^* = \omega^*/2\pi = 10$ Hz. NLC physical constants correspond to the temperature $\sim 20°C$.

Experimental values of the coefficient $A_{\ddot{\xi}}$ in Figure 4(b) are related to the sensors, filled with N-8 and differ by the membrane rigidity (that is the value of f^*) and NLC column height H. The symbol 1 corresponds to metal membrane with $f^* =$ 10 Hz ($d = 10^{-4}\ m$, $H = 0.5\ m$); 2, to metal membrane with $f^* = 100$ Hz ($d =$ $10^{-4}\ m$, $H = 0.1\ m$); 3, to lavsan one with $f^* = 1.6$ Hz ($d = 10^{-4}\ m$, $H = 0.01$ m), their thickness is about 20 μm.

Testing of these sensors was made in frequency band from 0.03 Hz up to 6 kHz by comparison with Brüel & Kjaer piezoceramic accelerometer data and with the amplitudes of oscillations, measured by means of a microscope. It is seen that just as for the variable pressure sensor it is possible by changing of the membrane rigidity to vary in some limits the frequency band, where the sensor has constant optical response to linear vibrational velocity. Agreement between experiment and theory is good.

ANGULAR VIBRATIONAL VELOCITY SENSOR

Scheme of the angular velocity sensor SC is presented in Figure 5. Here 1 is a ring-shaped chamber, 2 is a capillary.§

Operational principle of the sensor is the following: vibrational velocity $\Omega(t)$ at the expense of inertia forces $(1/4)\pi\rho H^2 \dot{\Omega}(t)$, depending on the whole length of the chamber, results in variable pressure at the SC input:

$$P(t) = \rho\pi H^2/4\omega\Omega(t). \tag{12}$$

The initial stage of signal conversion has the next form:

$$\varkappa_i(t) = \Omega(t) \rightarrow P(t). \tag{13}$$

Expression for the angular velocity conversion coefficient is:

$$A_\Omega = \pi N \rho H^2 d\ (\Delta n k_0 d(1/2 + m))^{1/2}/4\ \eta_{ef} L, \tag{14}$$

§ In the Figure it is shown the simplest one-turn SC; generally the chamber may consist of N turns.

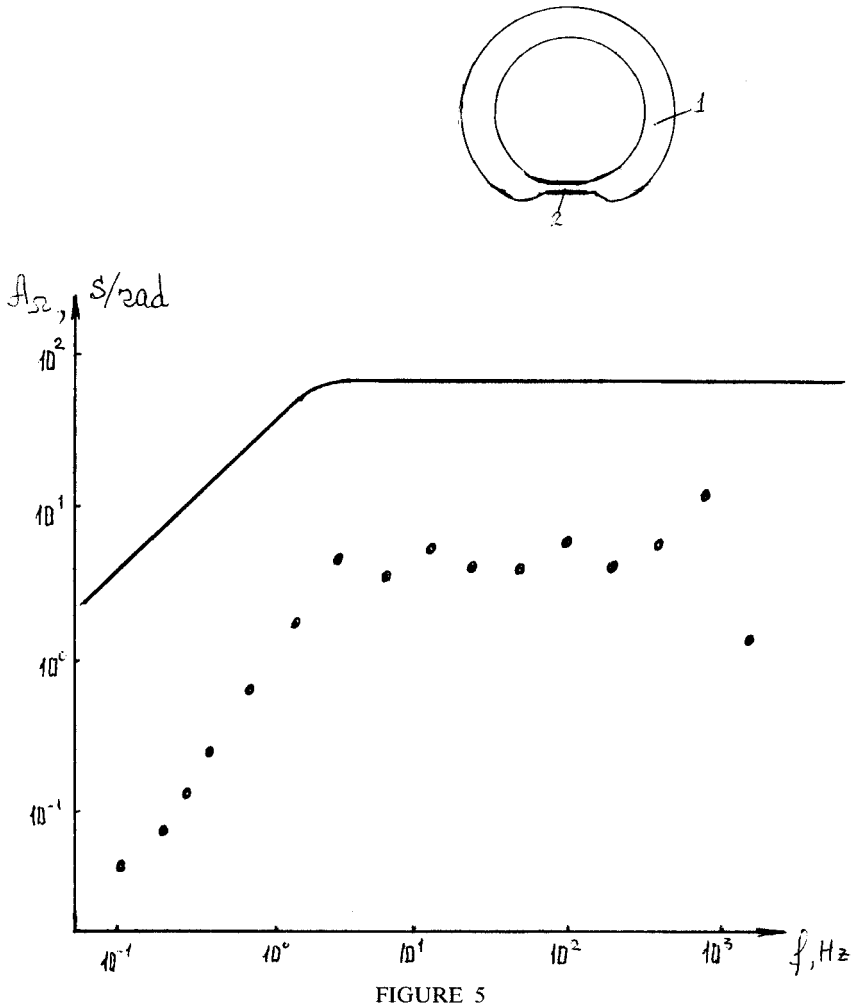

FIGURE 5

which is valid in the frequency band $\omega_L \ldots \omega_H$. Here N is the number of the ring-shaped chamber turns.

A plot in Figure 5(b) presents the coefficient values A_Ω calculated from Equation (14) for the sensor with the following geometrical dimensions: $d = 10^{-4}$ m; $L = 10^{-3}$ m; turns number is $N = 5$; $H = 10^{-1}$ m; NLC constants are taken at the temperature $\sim$ 20°C.

In that Figure there are also illustrated the results of preliminary testing of the sensor, filled with N-8, in the frequency band 0.1 . . . 1000 Hz, carried out by comparison with visual control of rotating motion of a platform, where the sensor was placed. Their deviation from the theory is caused by the membranes and small inner diameter of the chamber.

Let us point out one method to form in the sensor SC the initial stationary orientational distortion of such a sort: $\varphi_0(z) = \text{const}(2z/d)$, providing the conversion

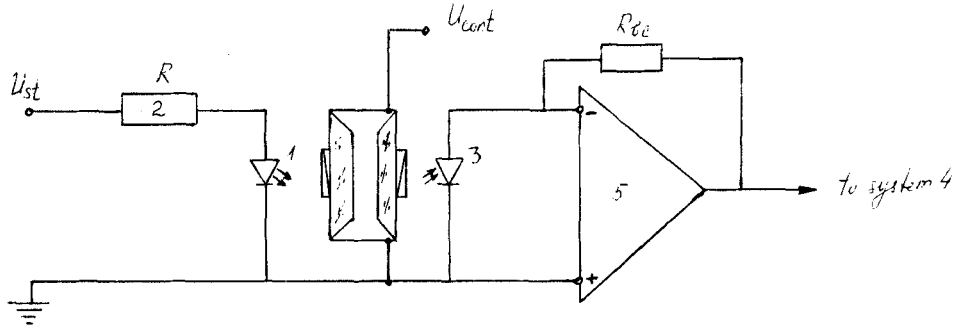

FIGURE 6

linearization.[‖] (Here φ_0 is an angle of the director tilt from the layer normal, coincident with Z axis). All the testings were fulfilled with the sensors, where the necessary NLC orientation was created by longitudinal electric field at the expense of the inverse flexoelectric effect.[4] By variation of a voltage u_{contr}, applied to the membranes (see Figure 6 where it is shown the sensor electric scheme), we managed to modify profile of the stationary distortion of NLC molecular orientation in the SC.

All the sensors considered above have one common feature: light-emitting diodes and photodiodes are built in the device body and connected with registrating and processing equipment by multicored electric cable. The typical electric scheme is presented in Figure 6. Stabilized current $I \simeq 50$ mA feeds light-emitting diode 1 through resistor 2 (~100 Ohm). The reading light flow passes through the SC and falls at photodiode[3], where it is transformed to a photocurrent. The latter is converted to a voltage u_{out}, which is transferred to registering and processing system 4. This output voltage is related with light intensity $I(t)$, incident at photodiodes, as follows:

$$u_{out} = \eta I(t) R_{bc}, \tag{15}$$

where η is quantum effectiveness of the photodiode, R_{bc} is back coupling resistance in operational amplifier circuit.

In order to determine the value of A_i we find while testing the voltage ratio $u_{\sim}/u_{=}$, corresponding to variable and constant components of the optical signal $I(t)$. Then we normalize the external action value to this voltage ratio.

It should be noted that dynamic range Δ of the sensor, using the optical scheme of information reading from the SC, is restricted by light shot noise. If the latter exceeds thermal noise of the back coupling resistance R_{bc} and operational amplifier, then the value of Δ in frequency band Δf is determined from the expression:

$$\Delta = 10 \lg(u_{=}/2eR_{bc}\Delta f). \tag{16}$$

‖ It is shown in Reference 2 that quasilinear signal conversion condition is reduced to creation in the plane section of the capillary of a stationary orientational distortion, coincident with its dynamic profile in the oscillating flow.

Here e is electron charge, $u_{=}/R_{bc}$ - photocurrent. In our testing, where $u_{=}/R_{bc}$ reached the value of $3 \cdot 10^{-5} A$ ($R_{bc} = 3 \cdot 10^5$ Ohm), the dynamic range is to be no less than 140 dB in 1 Hz band. However in real conditions different noises and energy losses, both optical and electric ones, reduce it to 100–120 dB. Therefore it is possible to estimate a threshold signal for any of the values being measured by the following expression:

$$\varkappa_{i_{\text{thr}}} = (10^{-5} \ldots 10^{-6}) A_i^{-1}. \tag{17}$$

As it was shown in preliminary study, NLC own noises spectral structure in the SC is so that mainly they are concentrated in frequency region $\omega < \omega_L$ and their spectral density reduces as $1/\omega^2$. Therefore the dynamic range of the sensors is not restricted by NLC noises at frequencies $\omega >> \omega_L$ and may reach 120–140 dB in 1 Hz band. When $\omega < \omega_L$, the dynamic range may reduce to 80–100 dB in 1 mHz band, if measures are not taken to select NLC layer thickness and to optimize the reading optical system. Thus, Equation (17) gives rather correct estimation of the threshold signal value, if the latter is taken in the band $\Delta f = 0.01\, f_0$, where f_0 is the middle frequency of the spectrum being investigated. Corresponding calculations result in the following threshold signal values of NLC sensors:

—variable pressure $10^{-5} \ldots 10^{-4}$ Pa;

—temperature fluctuations $10^{-7} \ldots 10^{-6}$ K;

—linear velocity $10^{-10} \ldots 10^{-9}$ m/s;

—angular velocity $10^{-8} \ldots 10^{-7}$ rad/s.

These experimental data were obtained in the sensors testing at laboratory benches, where one or another type of action was imitated. At the same time the sensors have also registered the corresponding parameters fluctuations, caused by natural effects or by influence of the factors, related with human activities (transport, industry, community noises). For example, in Figure 4(c) there are presented the data of the linear vibrational velocity sensor, obtained in the evening in frequency band 1 . . . 20 Hz. Strong discrete components of the spectrum are related to nearby metro line, different engines functioning and industrial noises.

In conclusion we note, that the developed NLC sensors, based on the effect of light polarization modulation, possess from our point of view the following considerable advantages: wide range (5–6 decades), low threshold signal levels, construction simplicity, low weight and small dimensions, compatibility with modern elements base of optical instrument-making, possible inmonochromaticity of the reading radiation ($\Delta\lambda_0/\lambda_0 \simeq 10^{-1}$), ability to adapt to variations of the parameters static values.

References

1. A. Kapustin and O. Kapustina, *Acoustics of Liquid Crystals* (Nauka, Moscow, 1985).
2. O. Kapustina and V. Reshetov, *Akust. Zhurnal*, **37**, 2 (1991).
3. T. Hayasaka, *Electroacoustics* (Mir, Moscow, 1982).
4. P. G. de Gennes, *The Physics of Liquid Crystals* (Clarendon Press, Oxford, 1974).